

Velocity covariance in the presence of anisotropic time correlated noise and transient events in GPS time series



Matthias Hackl^{a,*}, Rocco Malservisi^b, Urs Hugentobler^c, Yan Jiang^d

^a Department of Earth and Environmental Sciences, Ludwig-Maximilians-Universität, Theresienstr. 41, 80333 Munich, Germany

^b Department of Geology, University of South Florida, 4202, E. Fowler Avenue, SCA528, 33620 Tampa, FL, USA

^c Institute for Astronomical and Physical Geodesy, Technische Universität München, Munich, Germany

^d Jet Propulsion Laboratory, MS 238-600, 4800 Oak Grove Drive, Pasadena, CA 91109, USA

ARTICLE INFO

Article history:

Received 29 March 2013

Received in revised form 29 August 2013

Accepted 30 August 2013

Available online 17 September 2013

Keywords:

GPS time series

Colored noise

Transient event

Slow slip event

ABSTRACT

The presence of un-modeled transient events in GPS time series significantly influences the estimate of the noise characteristics. In particular, GPS time series affected by transient events with a preferential geographical orientation are affected by a regional pattern of anisotropic noise. We provide a method to derive the covariance of GPS velocities in the presence of time-correlated noise based on the Allan variance of the rate that can account for this anisotropy. The velocity variance is calculated for different directions, allowing for the detection of direction-dependent noise properties. The resulting covariance provides realistic estimates for the uncertainties of GPS derived surface velocities and is of particular interest for the analysis of time series affected by transient signals. We show that GPS sites in subduction zones experiencing slow slip events (SSEs) exhibit a significant component of time correlated “noise” in the direction of the SSE motion and that the velocity confidence ellipses are highly eccentric in this direction. The time correlation of the noise of these sites is significantly reduced after modeling and subtracting SSEs from the time series with a concomitant reduction of the anisotropy of the estimated velocity uncertainties.

© 2013 Elsevier Ltd. All rights reserved.

1. Introduction

GPS position time series provide an outstanding tool to measure crustal motion and deformation (e.g. Dixon, 1991; Segall and Davis, 1997; Ruegg et al., 2002; Jin et al., 2013). The availability of longer time series and the enhanced data quality allow for improved analyses of time dependent effects in deforming continental zones. These analyses may provide insights to the seismic cycle and provide constraints on parameters such as the rheology of the crust and the underlying asthenosphere (e.g. Malservisi et al., 2001, 2003a,b; Schmalzle et al., 2006; McCaffrey et al., 2007; Perfettini and Avouac, 2007; Bürgmann and Dresen, 2008).

GPS time series are also subject to many different kinds of time correlated noise, which is caused by non-stationary stochastic processes that are not considered to be part of the (modeled) signal. Its various sources include for example multipath, clock and orbit errors, and ionospheric and tropospheric effects. Usually,

those processes are not assessed individually, but their cumulative effect on the time series and the subsequent measures like site velocity are quantified through the application of error models that account for time correlation (Johnson and Agnew, 1995; Zhang et al., 1997; Mao et al., 1999; Williams et al., 2004; Langbein, 2008; Montillet et al., 2012; Olivares and Teferle, 2013). It is generally agreed upon by these authors that the time correlated noise in GPS time series can be approximated by one or more independent components of power law noise that is characterized by the power law index ν . Extensive work on the stochastic models underlying GPS time series has been carried out by Jin et al. (2005, 2010).

Additionally, networks of GPS sites may also be affected by transient events such as post-seismic deformation or slow slip events (SSE) (e.g. Wdowinski et al., 1997; Dong et al., 2006). The effect of transient events on the time series is very similar to the addition of time correlated noise, posing the problem of separating these signals from noise and correctly estimating velocity uncertainties (e.g. Williams, 2003a,b; Hackl et al., 2011). One way to address this problem has been introduced by Ji and Herring (2011), who were able to identify transient signals in GPS time series from the Aku-tan volcano by state estimation and principal component analysis. Ji and Herring (2013) expanded this algorithm and successfully tested

* Corresponding author. Tel.: +49 89 2180 4206.

E-mail addresses: hackl@geophysik.uni-muenchen.de (M. Hackl), rocco@usf.edu (R. Malservisi), urs.hugentobler@bv.tu-muenchen.de (U. Hugentobler), yjiang@caltech.edu (Y. Jiang).

it with GPS time series affected by the 1999 Hector Mine earthquake and ground water changes. Granat et al. (2013) presented a pure statistical approach to detect unmodeled signals in GPS time series.

Transient events in GPS time series are very common. They can result from a variety of processes such as post seismic deformation (e.g. Savage and Lisowski, 1998; Perfettini and Avouac, 2007; Hackl et al., 2009; Hammond et al., 2010), present day ice mass loss (e.g. Yang et al., 2013), volcanic deformation (e.g. Dzurisin, 2003; Saballos et al., 2013), anthropogenic deformation (e.g. Bawden et al., 2001), atmospheric processes (e.g. Jade and Vijayan, 2008 and references therein), tropospheric processes (e.g. Jin et al., 2008), or variable amplitude seasonal signals (Davis et al., 2012) and commonly affect GPS time series. A prominent tectonic mechanism that occurs at many subduction type plate boundaries and results in a deviation from a linear trend in GPS time series is the so-called slow slip event (SSE) (e.g. Hirose et al., 1999; Dragert et al., 2001). During SSEs some of the strain accumulated during the inter-seismic period is released by aseismic slip at weaker parts of the plate interface for a time period varying from days to months (see review in Schwartz and Rokosky, 2007). To first order, SSEs manifest themselves as quasi-periodic offsets in GPS time series (e.g. Szeliga et al., 2008; Schmidt and Gao, 2010; Jiang et al., 2012). Williams et al. (2004) and Hackl et al. (2011) showed that the presence of uncorrected offsets in a time series can be misinterpreted as a higher time correlation in the noise. For example, a time series affected by simple white noise containing an offset appears to contain a significant amount of random walk noise.

Transient signals that are related to tectonic processes are often affecting a larger region and can influence multiple GPS time series within an area in a similar way and even in a preferred direction. For example, post-seismic deformation affects a regional network in a well defined pattern. If the presence of the transient signal is not known a priori or is not accounted for in the signal analysis, it will be interpreted to be part of the ‘noise’ of the resulting time series. If the transient signal is occurring in a particular geographical direction, the inferred ‘noise’ content of a corresponding time series not corrected for the transient would not have the same characteristics in all the directions, but show some sort of anisotropy. The direction mostly affected by the un-modeled transient event would appear to have a noise content that is more time correlated, which results in a larger apparent uncertainty in this particular direction. To analyze this behavior we developed an algorithm based on the Allan variance of the rate (AVR) (Hackl et al., 2011) that evaluates the characteristics of time correlated noise for any chosen direction. The AVR provides the rate variance as a function of time span τ through the variance of the rate differences of consecutive bins of length τ of the time series. Note that any algorithm that provides noise parameters of a GPS time series that is affected by time correlated noise might also be used instead of the AVR. Along with the noise parameters this algorithm provides the variance and covariance of the rate in the presence of colored (time correlated) noise that comprises different noise characteristics for different directions. We apply this algorithm to two GPS networks known to be affected by SSEs and study the possibility to utilize it to evaluate models of SSE-induced surface deformation.

2. Directional noise analysis

GPS time series provide the temporal variation of the antenna position and can be interpreted as the sum of a long term trend (linear motion), shorter term motion (annual signals, offsets, transients, etc.), white noise, and colored noise. These components have to be separated and quantified in order to model and analyze any underlying process and to assign proper error bars on the

measurements. In general, if time dependent effects are not explicitly included in the signal analysis, they are implicitly considered to be part of the noise. Here we focus on the analysis of the noise in order to estimate the uncertainty of the secular rate, assuming that the time series have been corrected for known time dependent effects.

Uncertainties are defined by the standard deviation σ , which is derived from the variance σ^2 and provides a confidence interval. In the following we assume only Gaussian distributed noise and refer to the standard deviation as the uncertainty. In the two dimensional case the confidence interval is represented by the confidence ellipse or error ellipse (in three dimensions the error ellipsoid) and it is usually displayed as the 95% confidence ellipse. In a similar way, the 2d representation of the variance is called variance ellipse but, unlike the confidence ellipse, for most applications it does not have a direct interpretation in physical or statistical terms.

Following Strang and Borre (1997) the horizontal velocity variance can be expressed by the covariance matrix

$$\Sigma = \begin{pmatrix} \sigma_1^2 & \sigma_{12} \\ \sigma_{12} & \sigma_2^2 \end{pmatrix} \quad (1)$$

where σ_1^2 and σ_2^2 are the variances in x_1 and x_2 direction and σ_{12} is the covariance. This is a positive semi-definite matrix, thus it can be diagonalized by non-negative diagonal elements σ_{max}^2 and σ_{min}^2 and geometrically represented as the variance ellipse.

According to the law of error propagation (e.g. Bevington and Robinson, 2003), the velocity variance in a direction φ defined by the unit vector $\vec{\Phi} = (\cos \varphi, \sin \varphi)^T$, is expressed by

$$\begin{aligned} \sigma^2(\varphi) &= (\cos \varphi, \sin \varphi) \begin{pmatrix} \sigma_1^2 & \sigma_{12} \\ \sigma_{12} & \sigma_2^2 \end{pmatrix} \begin{pmatrix} \cos \varphi \\ \sin \varphi \end{pmatrix} \\ &= \sigma_1^2 \cos^2 \varphi + 2\sigma_{12} \cos \varphi \sin \varphi + \sigma_2^2 \sin^2 \varphi \end{aligned} \quad (2)$$

This result can also be obtained by pure geometrical considerations based on the confidence ellipse. The principal semi-axes of the confidence ellipse represent the maximum and minimum velocity uncertainties σ_{max} and σ_{min} , or multiples of them. In the case of a two dimensional Gaussian distribution the probability of a velocity to fall inside the confidence ellipse can be calculated by

$$W = 1 - e^{-\frac{1}{2}k^2}, \quad (3)$$

where k indicates the multiple of σ that underlies the confidence ellipse (e.g. Hoover, 1984).

If the squares of σ_{max} and σ_{min} are the entries of the diagonalized form of Σ , the velocity uncertainty in any direction φ is given by the projection of the ellipse in that direction (Fig. 1). Thus the velocity uncertainty $\sigma(\varphi)$ is identical to the support function of an ellipse, the so-called pedal curve:

$$\sigma(\varphi) = \sqrt{\sigma_{max}^2 \cos^2(\varphi - \alpha) + \sigma_{min}^2 \sin^2(\varphi - \alpha)} \quad (4)$$

where α is the angle between x_1 -axis and the major semi-axis of the ellipse. This pedal curve is the locus of points, where any line from the origin intersects a perpendicular line that is tangent to the ellipse. It can be shown (e.g. Strang and Borre, 1997) that Eq. (4) is also equivalent to Eq. (2) if Σ is not diagonalized. Note that this basic relationship between covariance and uncertainty in any direction assumes a (two or three dimensional) Gaussian distribution, but is independent from the characteristics of the underlying (colored) noise.

The position of the antenna at any epoch can be projected into the chosen direction defined by $\vec{\Phi}$ by the dot product of the position vector and $\vec{\Phi}$. In particular, in the horizontal 2d case, the east and north components of the position time series can be used to compute the projected position in any given direction φ at each time.

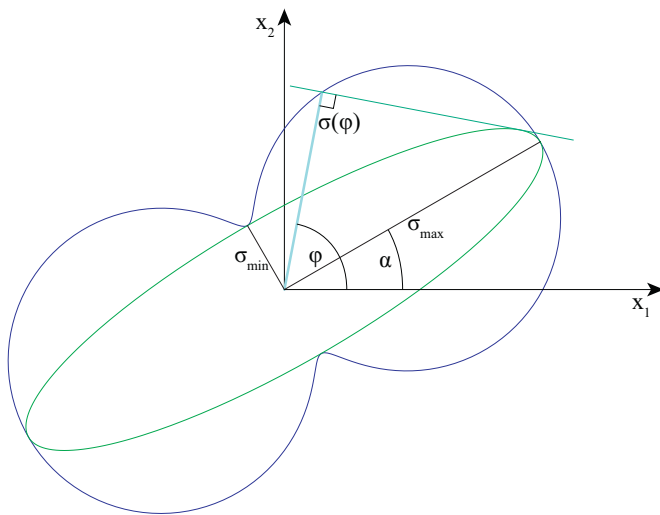


Fig. 1. Confidence ellipse (green) and corresponding support function (blue). (For interpretation of references to colour in this figure legend, the reader is referred to the web version of this article.)

The resulting time series can be used to calculate the corresponding velocity variance $\sigma^2(\varphi)$. If the velocity variance is known for at least three different horizontal directions φ , the full horizontal covariance matrix of the velocity can be obtained by inverting Eq. (2). Of course, this analysis can easily be extended to three dimensions, considering six unknowns and Σ being a 3×3 matrix that is represented by an ellipsoid. Due to the law of error propagation the horizontal confidence ellipse is the projection of this 3d ellipsoid onto the horizontal plane.

In order to derive the horizontal covariance matrix we project the east and north components of a position time series into at least three different directions φ obtaining time series $\xi_\varphi(t)$. Then the velocity variance $\sigma^2(\varphi)$ is calculated for each time series by applying the AVR (Hackl et al., 2011) and fitting an adequate error model. In this way it is possible to obtain different time correlation parameters for different directions. Finally, the covariance matrix is obtained by fitting Eq. (2) to the different velocity variances. This process is shown in more detail in Fig. 2.

In this work we focus on the application of the method to networks that are experiencing transients with a strong directivity in order to point out the sense in doing so. Nevertheless, the method was also tested and applied to the TrigNet GPS network of South Africa. It is worthwhile mentioning that the method provided reasonable rate uncertainty ellipses that were not very eccentric for most of the sites with random orientations.

3. Time correlated noise and velocity covariances in the Costa Rican Nicoya network

We analyzed the time series computed by Jiang et al. (2012) of twelve continuous GPS sites in Costa Rica. The network was initiated in 2002 to study strain accumulation of slow slip events in the adjacent subduction zone (Outerbridge et al., 2010) and was completed in 2008. GPS data were processed to produce non-fiducial daily solutions with the Jet Propulsion Laboratory (JPL)'s software GIPSY-OASIS 6.1.2 using the standard precise point-positioning (PPP) analysis strategy described by Zumberge et al. (1997). Data were analyzed using non-fiducial final orbits, clocks, and Earth orientation parameters provided by JPL. Ocean loading correction are modeled using FES2004 ocean loading coefficient from Onsala Space Observatory. VMF mapping function were used for nominal tropospheric values and mapping. Wet tropospheric delay was modeled with gradient parameters solved as random walk

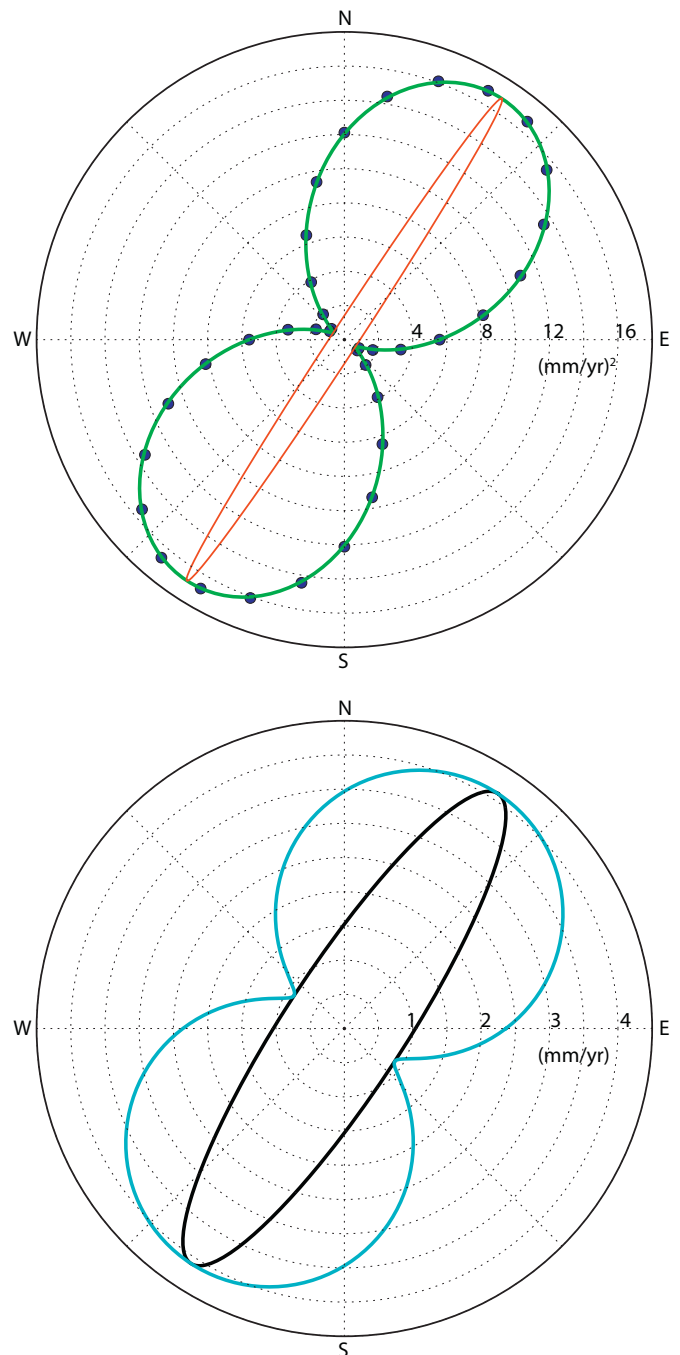


Fig. 2. Horizontal velocity variances (top) of site GRZA based on a white noise plus power law noise error model. Blue dots represent the estimated variances for the different directions. These variances have been fitted (green curve) using Eq. (2). Note, that the corresponding variance ellipse (red curve) represents the variance and not the uncertainty. The black ellipse (bottom) represents the 1σ confidence ellipse. The blue curve is the pedal curve and represents the actual 1σ uncertainty in any direction. (For interpretation of references to colour in this legend, the reader is referred to the web version of this article.)

(Bar-Sever et al., 1998). Ambiguity resolution was solved using the single receiver phase ambiguity resolution algorithm of Bertiger et al. (2010). The fiducial-free daily solutions were transformed into the International Terrestrial Reference Frame 2008 through a seven-parameter transformation using parameters provided by JPL.

During the period from 2002 to 2011 different SSEs close to the Nicoya peninsula were identified by Brown et al. (2005, 2009), Tryon (2009), Outerbridge et al. (2010), Davis et al. (2011), Walter

et al. (2011), Jiang et al. (2012). The surface deformation and fault slip of five of the observed SSEs was modeled by Jiang et al. (2012). To analyze the effects of SSEs on the estimation of secular rate uncertainties, we perform the previously described analysis on both the raw GPS time series and time series corrected for the modeled surface deformation caused by the SSEs (Jiang et al., 2012). Note that a simple sinusoidal model was applied for the annual and semiannual signals in the velocity model. Nevertheless, it cannot be ruled out for any of the time series analyzed in the context of this study to contain colored noise caused by processes other than the SSEs. In theory, the analysis of the time series for at least three different directions is necessary to derive the 2d covariance. However, to test the stability of the model, the horizontal components of the time series of each site were projected into 18 different horizontal directions (one every 10°). Then the AVR of the obtained time series was calculated for every direction. The variance of the rate for each direction was computed by fitting the AVR applying two different error models, (1) “white noise + flicker noise + random walk” and (2) “white noise + power law noise”. These variances are then fitted using Eq. (2) to obtain the 2d velocity covariance for the two different error models. As an example Fig. 2 (top) shows this process for the uncorrected time series for site GRZA, applying the “white noise + power law noise” error model. The blue dots correspond to the variances of the time series projected into the different directions. Using Eq. (2) the green curve is fitted to these values to obtain the three components of the variance. The principal components of the variance are graphically represented by the red ellipse. The corresponding 1σ confidence ellipse is presented in the lower panel of Fig. 2 (black curve), while the function representing the projection of the uncertainty into all horizontal directions (pedal curve) is shown in blue.

In the case of the “white noise + power law noise” error model, one of the parameters we solve for is the spectral index ν . This index characterizes the power spectrum of the noise ($\nu=0$ indicates white noise, $\nu=-1$ flicker noise, and $\nu=-2$ random walk) and is estimated independently for each direction. As an example Fig. 3 shows the different spectral indices as a function of the azimuth for the site GRZA for the uncorrected (top) and corrected (bottom) time series. Usually, GPS sites that are not affected by transients exhibit a power law noise that is close to flicker noise ($\nu=-1$, green curve) (Mao et al., 1999; Langbein, 2008; Hackl et al., 2011). In this case the uncorrected time series presents a much lower spectral index (higher time correlation) in particular in the direction corresponding to the surface displacement induced by the identified SSEs. The time series corrected for the transients shows less time correlation and a more isotropic behavior of the spectral index and also the error ellipse.

The results from the analysis of the Costa Rican sites are summarized in Tables 1 and 2, and in Figs. 4–6. It is interesting to note that the uncertainty estimates of the two different error models produce very similar results in terms of azimuth and magnitude of the confidence ellipse for most sites (black and red ellipses in Fig. 4, blue and orange ellipses in Fig. 5). The few cases with significantly different results correspond to sites where the chosen error model does not fit the AVR very well.

The direction of the inter-seismic secular rate coincides well with the relative plate motion direction of the fore-arc sliver migration (LaFemina et al., 2009; Outerbridge et al., 2010; Jiang et al., 2012). For the uncorrected time series, the sites BON2, GRZA, IND1, LEPA, LMNL, PUMO, and QSEC show very eccentric velocity confidence ellipses with the major semi-axis oriented SW-NE. Their direction is rather normal to the plate boundary, approximately 20° more to the east with respect to the inter-seismic velocities. This is probably related to regional strain partitioning between a nearly normal relative motion at the subduction zone and a trench parallel motion of fore-arc sliver. Indeed, the larger principal axis of the

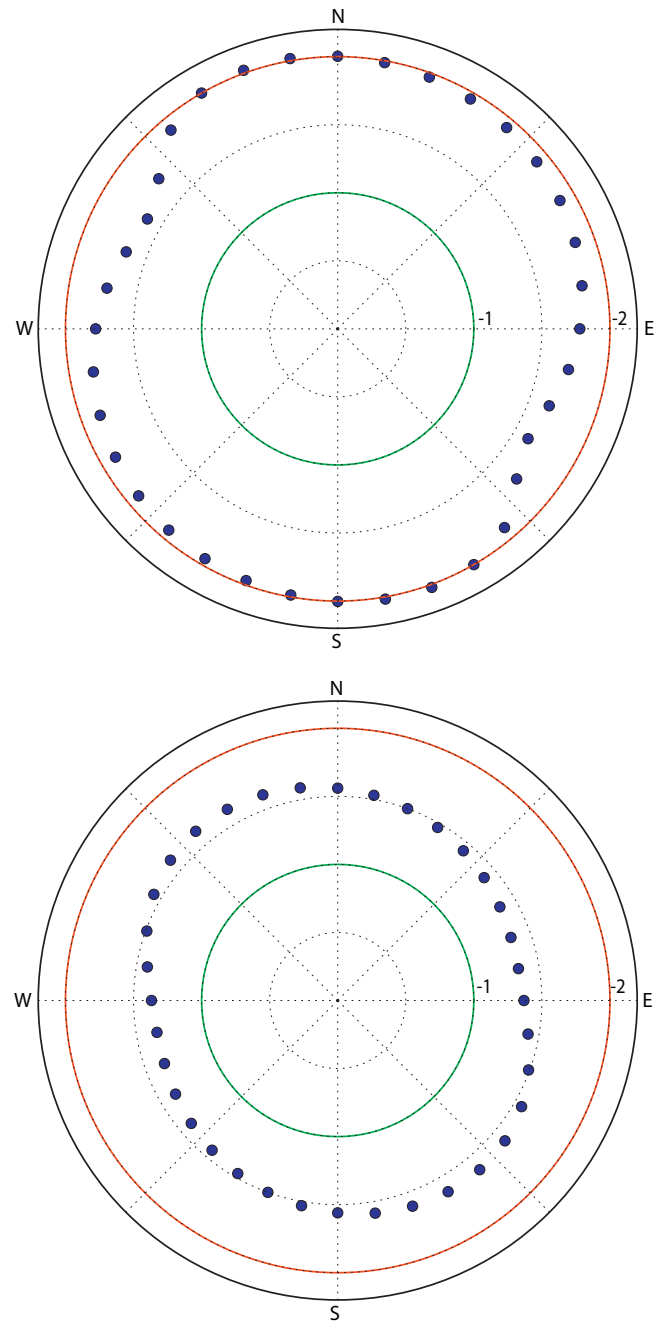


Fig. 3. Spectral indices of GRZA (blue dots) that were estimated along with the variances (see Fig. 2). Values far from the origin represent high time correlation. The green circle corresponds to flicker noise, the red circle to random walk. The spectral indices have been estimated from the raw time series (top) and from the residual time series after correcting for the SSEs (bottom). (For interpretation of references to colour in this figure legend, the reader is referred to the web version of this article.)

error ellipses seem to be oriented in the direction of the modeled SSEs surface displacement (orange vector in Fig. 4).

It is also important to note that all the sites with highly anisotropic uncertainties have a large component of random walk (or very low spectral indices) in the direction corresponding to the larger principal axis of the error ellipse. As already stated, offsets and velocity changes in time series result in a noise pattern that is similar to highly time correlated noise (Williams, 2003b; Hackl et al., 2011). If un-modeled offsets occur in some preferred direction, an increased time correlation and, for a given time series

Table 1

Estimated noise magnitudes and 1σ velocity uncertainties in principal axis directions based on a “white noise + flicker noise + random walk” error model of continuous GPS sites in Costa Rica. sse corresponds to the time series corrected for surface displacement induced by SSEs.

Site	Azimuth ° cw from N		Principal axis	σ_v (mm/yr)	sse	a_{wn} (mm \sqrt{d})	sse	a_{fl} (mm)	sse	a_{rw} (mm $/\sqrt{d}$)	sse
	raw	sse									
BON2	41.88	46.65	max	3.50	0.90	2.17	1.84	0.00	1.58	0.46	0.11
			min	0.65	0.56	1.85	1.80	1.36	1.40	0.07	0.06
GRZA	38.72	31.07	max	3.95	1.27	1.76	1.53	1.29	1.62	0.47	0.14
			min	1.06	0.71	2.05	2.09	0.71	0.88	0.12	0.08
HATI	45.05	37.73	max	1.35	0.31	1.83	1.78	1.15	1.19	0.15	0.00
			min	0.23	0.26	1.92	2.04	1.15	0.98	0.00	0.00
HUA2	9.66	63.6	max	1.46	0.25	1.91	1.58	0.96	1.67	0.23	0.00
			min	0.01	0.17	1.67	1.89	1.55	1.10	0.00	0.00
IND1	45.22	50.15	max	1.17	0.31	1.94	2.17	2.35	2.09	0.17	0.00
			min	0.27	0.20	2.23	2.27	1.41	1.35	0.03	0.00
LEPA	28.38	36.52	max	3.29	0.32	1.83	1.57	0.00	1.24	0.39	0.00
			min	1.26	0.26	1.88	1.84	0.81	1.00	0.14	0.00
LMNL	39.44	-50.66	max	1.57	0.34	1.86	1.89	0.74	1.06	0.17	0.00
			min	0.01	0.30	1.84	1.81	1.17	0.94	0.00	0.00
PNEG	62.26	65.2	max	0.62	0.56	2.29	2.43	2.04	1.83	0.00	0.00
			min	0.42	0.41	2.39	2.41	1.38	1.35	0.00	0.00
PUJE	-0.66	-85.77	max	1.30	0.24	2.21	1.96	0.89	1.55	0.20	0.00
			min	0.53	0.19	1.93	2.12	1.59	1.21	0.07	0.01
PUMO	24.52	-79.83	max	2.83	0.39	1.77	1.65	0.00	1.20	0.29	0.00
			min	0.77	0.37	1.60	1.55	1.28	1.13	0.05	0.00
QSEC	29.93	28.78	max	3.62	1.27	2.11	1.64	0.00	1.66	0.43	0.14
			min	0.90	0.31	2.12	2.12	1.02	1.03	0.10	0.02
SAJU	51.28	62.12	max	3.38	0.57	1.73	1.71	1.20	1.43	0.32	0.00
			min	0.01	0.43	1.74	1.87	1.36	1.06	0.00	0.00

length, a larger uncertainty would be inferred in that particular direction.

The orientations of the major semi-axis of the uncertainty ellipses of the six above mentioned sites are in good agreement with the direction of the induced surface displacement due to the SSEs modeled by Jiang et al. (2012) (orange vectors in Fig. 4). The uncorrected time series for the stations HATI and PNEG present a similar pattern of the previous six stations but with a much more isotropic noise content. Their less eccentric error ellipses are compatible with the smaller surface deformation due to SSEs. Only HUA2 and PUJE show a different pattern with the major semi-axes oriented N-S.

This pattern can be related to the fact that these two sites lie in between two different patches that experience SSEs and present a large scatter of directions for the modeled SSE motions (Fig. 4). Nevertheless, it is important to note that an analysis of the vertical components of these two sites and discussion with Observatorio Vulcanológico y Sismológico de Costa Rica (Protti personal comm. December 2nd 2012) indicate that the time series are affected by the offset induced by a change of antenna in 2010 which is currently (March 2013) not reported in the corresponding log file. It is thus possible that some part of the anomalous orientation of the uncertainty ellipse can be due to this offset.

Table 2

Estimated power law indices and 1σ velocity uncertainties in principal axis directions based on a “white noise + power law noise” error model of continuous GPS sites in Costa Rica. “raw” indicates the results based on the original time series and “res” the results based on the residual time series, after subtracting the modeled SSEs.

Site	Azimuth ° cw from N		Principal axis	σ_v (mm/yr)	sse	Power law	
	raw	sse				index	raw
BON2	37.8	41.57	max	4.30	0.82	-2.16	-1.42
			min	0.01	0.52	-1.28	-1.29
GRZA	33.15	14.83	max	4.10	1.12	-2.02	-1.62
			min	0.88	0.66	-1.61	-1.35
HATI	41.56	57.72	max	1.13	0.36	-1.60	-1.16
			min	0.30	0.11	-1.15	-0.57
HUA2	8.79	21.24	max	1.37	0.21	-1.91	-0.98
			min	0.23	0.12	-1.38	-0.74
IND1	46.53	40.79	max	0.94	0.28	-1.43	-0.93
			min	0.20	0.10	-0.93	-0.65
LEPA	26.98	6.08	max	3.88	0.33	-2.14	-1.04
			min	1.24	0.12	-1.82	-0.57
LMNL	44.59	70.46	max	1.58	0.13	-2.02	-0.56
			min	0.01	0.12	-1.18	-0.33
PNEG	42.96	65.73	max	0.73	0.24	-1.13	-0.51
			min	0.34	0.14	-0.82	-0.36
PUJE	5.53	29.9	max	1.14	0.27	-1.80	-1.17
			min	0.01	0.08	-1.04	-0.64
PUMO	26.05	15.26	max	3.42	0.22	-2.32	-0.73
			min	0.47	0.15	-1.63	-0.48
QSEC	30.34	25.97	max	4.08	1.20	-2.14	-1.58
			min	0.01	0.39	-1.42	-1.20
SAJU	48.68	44.76	max	3.05	0.31	-1.82	-0.63
			min	0.01	0.13	-0.98	-0.32

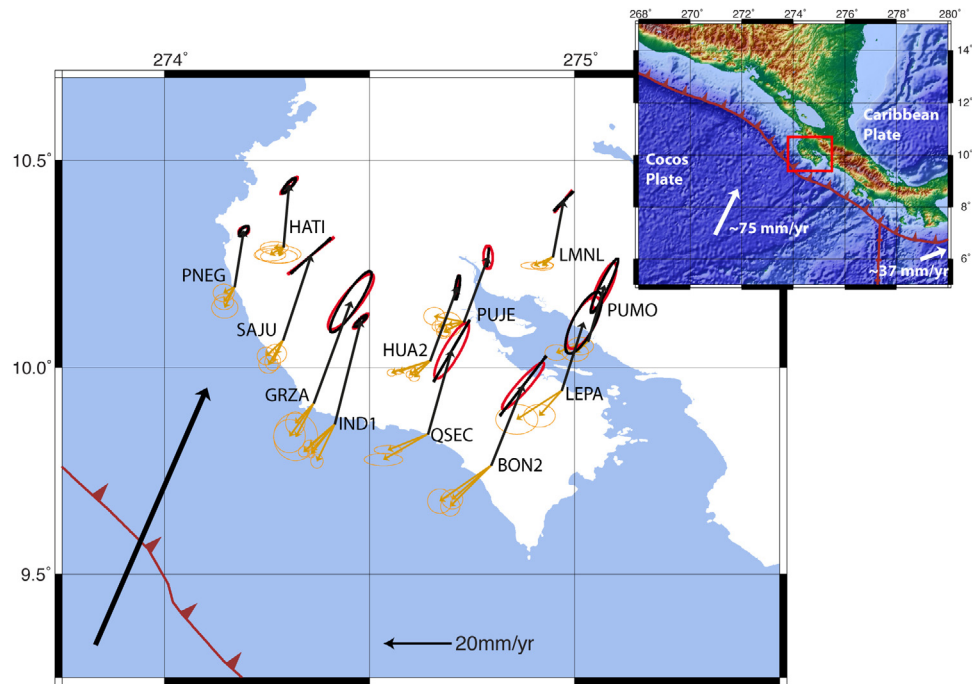


Fig. 4. Figure of the Nicoya peninsula, Costa Rica, with inter-seismic GPS velocity field. All velocities are with respect to a fixed Caribbean Plate. The figure shows 95% velocity confidence ellipses using the raw time series, where red ellipses are based on a “white noise + flicker noise + random walk” error model, and black ellipses on a “white noise + power law” error model. Orange arrows indicate horizontal displacements during the SSE according to Jiang et al. (2012). The large black arrow represents the MORVEL motion of Cocos with respect to Caribbean (DeMets et al., 2010). (For interpretation of references to colour in this figure legend, the reader is referred to the web version of this article.)

As seen for site GRZA (Fig. 3), if the modeled SSE surface displacements are subtracted from the time series, the spectral index and therefore the shape and dimension of the error ellipses are significantly affected. The analysis of the spectral index of the “white noise + power law noise” error model for the corrected time series shows values closer to flicker noise ($\nu = -1$) for all the directions

(Table 2 and Fig. 6). Similarly, in the case of the “white noise + flicker noise + random walk” error model, the uncorrected time series is exhibiting a direction with a significant amount of random walk noise, while after the correction flicker noise is prevalent in all the directions (Table 1). The velocity variances of the corrected time series do not indicate anymore the presence of a preferred orientation (Fig. 5) and the ellipses seem to become more isotropic (blue and orange ellipses) compared to the raw time series (black and red ellipses). Furthermore, the time correlation reduction in the estimated noise is reflected in significantly smaller error ellipses.

4. US Pacific Northwest, PANGA Cascadia network

If the presence of SSE in Costa Rica is the principal factor for the eccentricity of the confidence ellipses for uncorrected time series, a similar behavior should be observed in other regions affected by slow slip events such as the Cascadia subduction zone.

Among others, Dragert et al. (2001), Miller et al. (2002), Rogers and Dragert (2003) describe SSEs accompanied by non-volcanic tremor at this plate boundary, where the Juan de Fuca plate is subducted beneath the North American plate at a rate of ~ 38 mm/yr. Thirty four SSEs between 1997 and 2005 have been described by Szeliga et al. (2008) using GPS data. The events occurred at Puget Sound and south of the Sound down to $\sim 46^\circ$ North. The region is covered by ~ 600 continuously operating GPS sites providing the possibility to analyze the spatial distribution of transients.

We applied the same analysis we used for the Costa Rica sites to all time series of the PANGA (Pacific Northwest Geodetic Array¹) network with more than four years of data (Fig. 7). The PANGA GPS time series up to 2011.2991 have been processed with JPL orbits

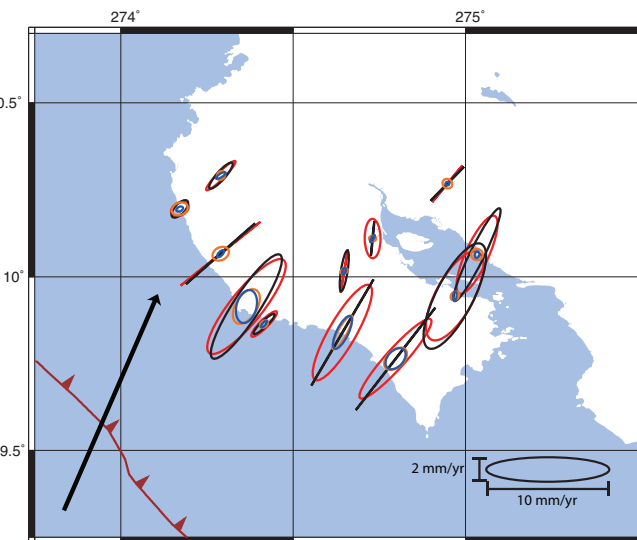


Fig. 5. 95% confidence ellipses of the velocities for different error models and for the raw and corrected time series. Black and red ellipses are the same as in Fig. 4 and correspond to the uncertainties calculated for the raw series. Orange and blue ellipses represent the 95% confidence ellipses of the rates (“white noise + flicker noise + random walk”: orange; “white noise + power law noise”: blue) based on the residual time series, after subtracting the SSE modeled by Jiang et al. (2012) from the time series. (For interpretation of references to colour in this figure legend, the reader is referred to the web version of this article.)

¹ <http://www.geodesy.cwu.edu/>, last accessed March 1st 2013

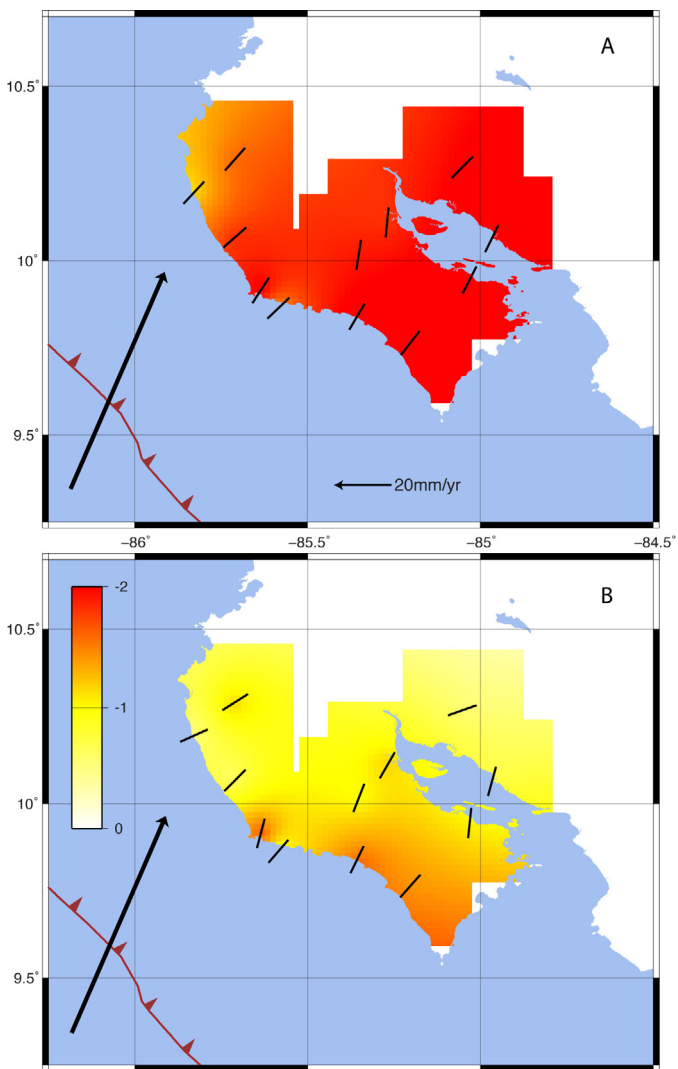


Fig. 6. Interpolated fields of the estimated spectral indices (see colorbar) in direction of the highest time correlation (black bars). A spectral index of -1 corresponds to flicker noise, -2 to random walk: (A) shows the spectral indices calculated from the cleaned time series (corrected for trends, offsets, annual, and semiannual signals) and (B) is based on time series that have additionally been corrected for modeled SSEs. (For interpretation of references to colour in this figure legend, the reader is referred to the web version of this article.)

using IGS05, and with IGS08 after that date. The PPP processing corrects for ocean loading, solid tides, pole tides and uses absolute phase center antenna calibrations for the ground and satellite antenna. PPP is performed using ionosphere-free combination of the observables (PC,LC) therefore the ionosphere is removed to first order. No second order ionosphere correction is applied. Inter-frequency and differential code biases are applied at the data editing step, before the PC and LC combinations are formed. No multipath correction is applied to the observables. No hydrological model is applied to either during the processing or post-processing.

As expected, an analysis using the uncorrected time series reveals similar results than the Costa Rica study. Many coastal sites show uncertainty ellipses that are significantly elongated in a direction almost perpendicular to the plate boundary. Interior sites have elongated ellipses more aligned with the relative plate motion direction. Uncertainty ellipses of sites further to the east, close to the volcanic arc are oriented mainly E-W again. Sites south and east of the area affected by SSEs, in general, show smaller uncertainties with randomly distributed principal axes. A more complex pattern

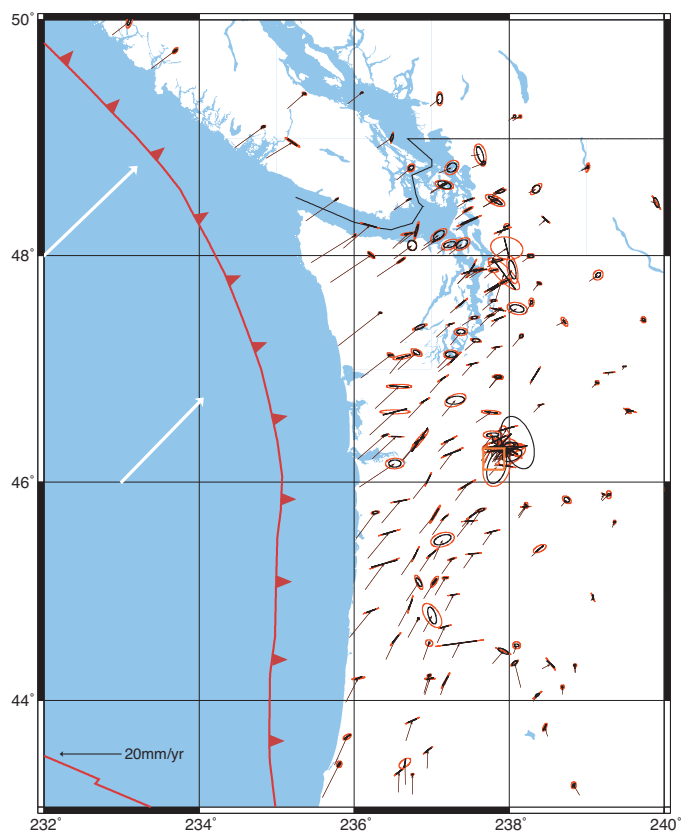


Fig. 7. PANGA GPS interseismic velocity field with 95% confidence ellipses calculated using a “white noise + power law noise” error model (black) and a “white noise + flicker noise + random walk” error model (red). Red arrows indicate plate motions with respect to stable North America. The orange rectangular indicates the position of Mount St. Helens. (For interpretation of references to colour in this figure legend, the reader is referred to the web version of this article.)

is present in the region of Mount St. Helens (square in Fig. 7). Since the volcanic activity is likely to mask the effects of SSEs, for this analysis we excluded the sites around Mount St. Helens.

The “white noise + power law noise” error model was employed again and the spectral indices of the power law noise were estimated along with the uncertainties. Fig. 8 shows an interpolation of the smallest spectral index (highest time correlation) and the corresponding directions. Fig. 8A shows the spectral index for detrended time series corrected for known offsets and filtered from annual and semi-annual signals but not corrected for SSEs. As for Costa Rica, instead of values close to flicker noise ($\nu = -1$) as generally expected for GPS sites, most of the sites affected by SSEs show at least a direction with an apparent time correlated noise close to random walk ($\nu = -2$).

The geodetic group at the Central Washington University (T. Melbourne pers. comm., 29 November 2011) measured the offsets in the time series caused by 20 SSEs between 1997 and 2011 and modeled the surface displacements caused by these events. The analysis of the spectral indices of the time series corrected for the modeled surface displacements and the measured offsets are presented in Fig. 8B and C, respectively. In both cases the time correlation of the noise in the regions affected by SSEs is reduced significantly. Some sites, however, show relatively high time correlations even after the correction for SSE displacements. In particular, the sites close to the coast of Puget Sound show a significant component of high time correlated noise. Apart from the obvious possibility of an incomplete correction of the effects due to SSEs, a very likely reason for high time correlated

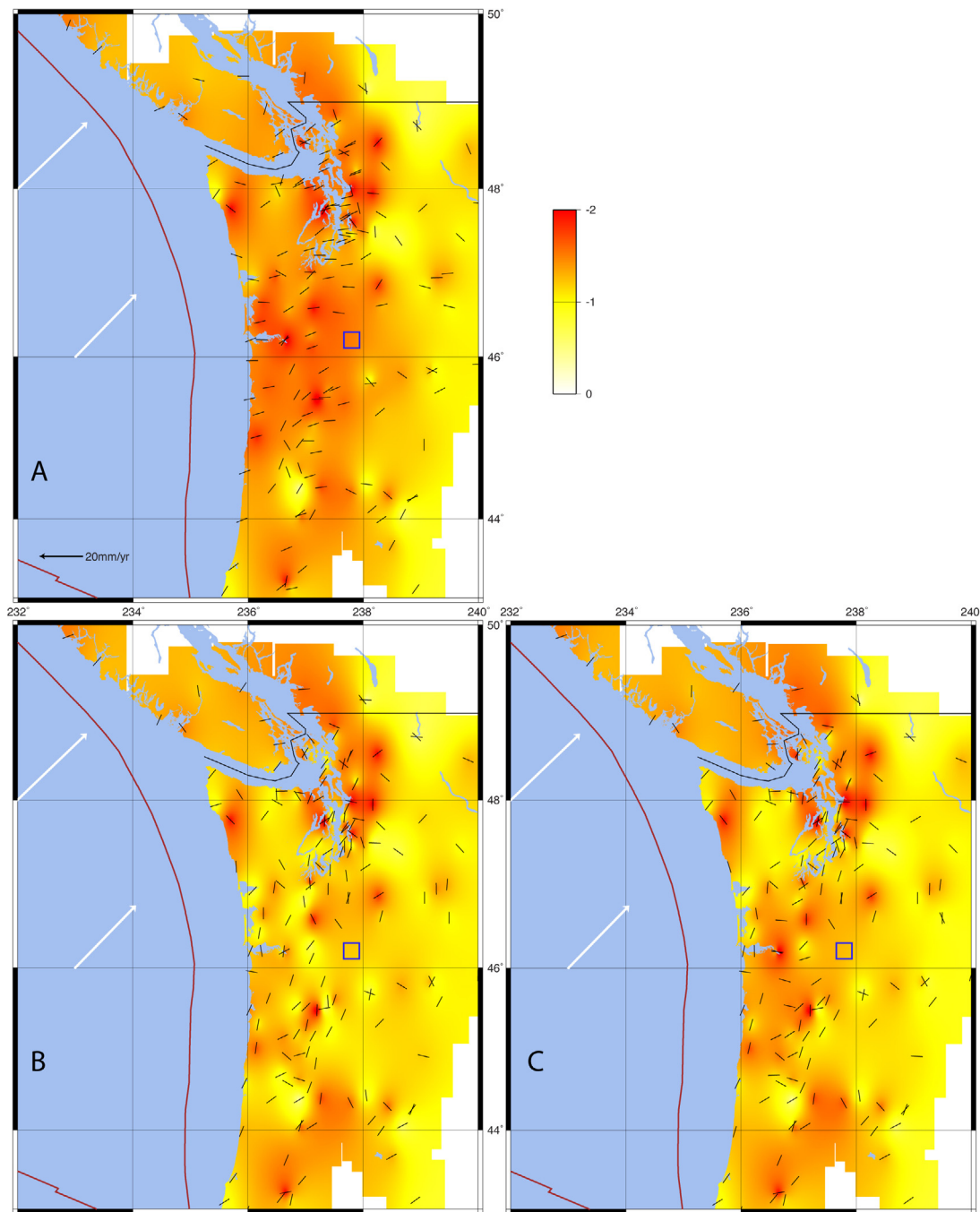


Fig. 8. Interpolated fields of the estimated spectral indices (see colorbar) in direction of the highest time correlation (black bars). (A) shows the spectral indices calculated from the cleaned time series (corrected for trends, offsets, annual, and semiannual signals). (B) is based on time series that have additionally been corrected for 20 modeled SSEs. (C) is based on time series that have been corrected for the measured offsets during the SSEs. (For interpretation of references to colour in this figure legend, the reader is referred to the web version of this article.)

noise in this region is the presence of transient effects due to the $M_w = 6.8$ Nisqually earthquake in 2001. It is intriguing that the region where the spectral index is not reduced to flicker noise is matching the area mostly affected by surface displacement during the earthquake very well (Bustin et al., 2004). This would also be the region mostly affected by post-seismic relaxation. It is very likely that the time correlated noise in these time series even after the SSEs correction do reflect this transient phenomena. Another cause of transient crustal deformation could be glacial isostatic adjustment that is not modeled in the time series and could lead to the presence of colored “noise” (James et al., 2000).

5. Conclusion

Many GPS time series are affected by time dependent (transient) signals. These signals can be caused by a variety of sources including tectonic related transient processes and time correlated noise. The analysis of transients provides insights to processes like post-seismic relaxation, SSEs, and volcanic deformation. If transient phenomena are not explicitly included in the analysis of the time series, they could result in apparent highly time correlated “noise” (similar to a random walk process). In particular, if the event is primarily affecting a given direction, it could lead to an estimation of large and highly eccentric velocity confidence ellipses.

In order to analyze the directional dependence of time correlated noise in GPS time series, we computed the velocity covariance of GPS time series. The full covariance of the secular rate of GPS time series is obtained by projecting the position time series into different horizontal directions. For each direction we apply the Allan variance of the rate to estimate the velocity variance. The variance for each direction is then fitted with Eq. (2) to compute the full variance of the secular rate. This method is easy to implement, accounts for time correlated noise, and allows for different noise characteristics for different directions.

The analysis of the time series of most GPS sites in Costa Rica and Cascadia not corrected for deformation induced by SSEs results in velocity confidence ellipses, which are strongly elongated in the direction of known SSE surface displacements. It also produces highly time correlated apparent “noise” in the same direction. The subtraction of the surface deformation associated with the transient behavior of SSEs from the time series results in confidence ellipses significantly less eccentric and spectral indices reduced to flicker noise. This indicates that SSEs account for a large portion of the apparent time correlated noise in the analyzed networks. More in general, un-modeled transient events with a strong preferred orientation will introduce some sort of apparent anisotropy in the time correlated noise suggesting that this analysis could be helpful to identify time series affected by unknown transient events.

To conclude, the examples of Costa Rica and Cascadia demonstrate the importance to account for the full covariance that takes into account colored noise. This is particularly true for regions that could be affected by transient signals. If the transient signal is not taken into account in the calculation of the secular rate and its uncertainty, it is critical to include colored noise in the full covariance analysis. Not including colored noise could lead to a biased interpretation of a spatially coherent velocity field as real secular rate coherency, while in reality it would be the apparent “noise” content (or the direction of the un-modeled transient event). The importance of the orientation of highly eccentric error ellipses due to anisotropic time correlation of the “noise” content can also be exemplified by the analysis of the residuals in slowly deforming regions. In these regions the deformation signal is often of the same magnitude as the uncertainty. In those cases the presence of a signal is inferred from a non-random distribution of the azimuth of the residuals (e.g. Plattner et al., 2007; Malservisi et al., 2013). While this is true in the case of circular error ellipses, a bias might be introduced in the case of spatially coherent eccentric error ellipses. In the latter case, the observed noise has a preferred direction implying that also the residuals could present a preferred orientation without to represent the true secular signal.

Acknowledgments

We used data of the Pacific Northwest Geodetic Array provided by the Central Washington University. We are grateful to Tim Melbourne and the geodetic group of Central Washington University for providing the surface displacement data due to the slow slip events. We would like to thank Tim Dixon for his comments that helped to improve this manuscript. This research was partially funded by the Bavarian Elite Network and the DFG grants BA1210/18-1, MA4163/1-2.

References

- Bar-Sever, Y.E., Kroger, P.M., Borjesson, J.A., 1998. Estimating horizontal gradients of tropospheric path delay with a single GPS receiver. *Journal of Geophysical Research: Solid Earth*, doi: 10.1029/97JB03534.
- Bawden, G.W., Thatcher, W., Stein, R.S., Hudnut, K.W., Peltzer, G., 2001. Tectonic contraction across Los Angeles after removal of groundwater pumping effects. *Nature*.
- Bertiger, W., Desai, S.D., Haines, B., Harvey, N., Moore, A.W., Owen, S., Weiss, J.P., 2010. Single receiver phase ambiguity resolution with GPS data. *Journal of Geodesy* 84, doi: 10.1007/s00190-010-0371-9.
- Bevington, P., Robinson, D., 2003. *Data Reduction and Error Analysis for the Physical Sciences*. McGraw-Hill Higher Education, McGraw-Hill, ISBN 9780072472271.
- Brown, J.R., Beroza, G.C., Ide, S., Ohta, K., Shelly, D.R., Schwartz, S.Y., Rabbel, W., Thorkwart, M., Kao, H., 2009. Deep low-frequency earthquakes in tremor localize to the plate interface in multiple subduction zones. *Geophysical Research Letters*, doi: 10.1029/2009GL040027.
- Brown, K.M., Tryon, M.D., DeShon, H.R., Dorman, L.M., Schwartz, S.Y., 2005. Correlated transient fluid pulsing and seismic tremor in the Costa Rica subduction zone. *Earth and Planetary Science Letters*, doi: 10.1016/j.epsl.2005.06.055.
- Bürgmann, R., Dresen, G., 2008. Rheology of the lower crust and upper mantle: evidence from rock mechanics. *Geodesy, and Field Observations*. Annual Review of Earth and Planetary Sciences, doi: 10.1146/annurev.earth.36.031207.124326.
- Bustin, A., Hyndman, R.D., Lambert, A., Ristau, J., He, J., Dragert, H., Van der Kooij, M., 2004. Fault parameters of the nisqually earthquake determined from moment tensor solutions and the surface deformation from GPS and InSAR. *Bulletin of the Seismological Society of America*.
- Davis, E., Heesemann, M., Wang, K., 2011. Evidence for episodic aseismic slip across the subduction seismogenic zone off Costa Rica: CORK borehole pressure observations at the subduction prism toe. *Earth and Planetary Science Letters* 0 (3–4).
- Davis, J.L., Wernicke, B.P., Tamisiea, M.E., 2012. On seasonal signals in geodetic time series. *Journal of Geophysical Research: Solid Earth*, doi: 10.1029/2011JB008690.
- DeMets, C., Gordon, R.G., Argus, D.F., 2010. Geologically current plate motions. *Geophysical Journal International*, doi: 10.1111/j.1365-246X.2009.04491.x.
- Dixon, T.H., 1991. An introduction to the global positioning system and some geological applications. *Reviews of Geophysics*, doi: 10.1029/91RG00152.
- Dong, D., Fang, P., Bock, Y., Webb, F., Prawirodirdjo, L., Kedar, S., Jamason, P., 2006. Spatiotemporal filtering using principal component analysis and Karhunen–Loeve expansion approaches for regional GPS network analysis. *Journal of Geophysical Research*, doi: 10.1029/2005JB003806.
- Dragert, H., Wang, K., James, T.S., 2001. A silent slip event on the deeper Cascadia subduction interface. *Science*, doi: 10.1126/science.1060152.
- Dzurisin, D., 2003. A comprehensive approach to monitoring volcano deformation as a window on the eruption cycle. *Reviews of Geophysics*, doi: 10.1029/2001RG000107.
- Granat, R., Parker, J., Kedar, S., Dong, D., Tang, B., Bock, Y., 2013. Statistical approaches to detecting transient signals in GPS: results from the 2009–2011 transient detection exercise. *Seismological Research Letters*, doi: 10.1785/0220130039.
- Hackl, M., Malservisi, R., Wdowinski, S., 2009. Strain rate patterns from dense GPS networks. *Natural Hazards and Earth System Sciences*.
- Hackl, M., Malservisi, R., Hugentobler, U., Wonnacott, R., 2011. Estimation of velocity uncertainties from GPS time series: examples from the analysis of the South African TrigNet network. *Journal of Geophysical Research*, doi: 10.1029/2010JB008142.
- Hammond, W., Kreemer, C., Blewitt, G., Plag, H.-P., 2010. Effect of viscoelastic postseismic relaxation on estimates of interseismic crustal strain accumulation at Yucca Mountain, Nevada. *Geophysical Research Letters*, doi: 10.1029/2010GL04279.
- Hirose, H., Hirahara, K., Kimata, F., Fujii, N., Miyazaki, S., 1999. A slow thrust slip event following the two 1996 Hyuganada earthquakes beneath the Bungo Channel, southwest Japan. *Geophysical Research Letters*.
- Hoover, W.E., 1984. Algorithms for confidence circles and ellipses. Technical Report NOS 107 C&GS 3, NOAA.
- Jade, S., Vijayan, M.S.M., 2008. GPS-based atmospheric precipitable water vapor estimation using meteorological parameters interpolated from NCEP global reanalysis data. *Journal of Geophysical Research*, doi: 10.1029/2007JD008758.
- James, T.S., Clague, J.J., Wang, K., Hutchinson, I., 2000. Postglacial rebound at the northern Cascadia subduction zone. *Quaternary Science Reviews*.
- Ji, K.H., Herring, T.A., 2011. Transient signal detection using GPS measurements: transient inflation at Akutan volcano, Alaska, during early 2008. *Geophysical Research Letters*, doi: 10.1029/2011GL046904.
- Ji, K.H., Herring, T.A., 2013. A method for detecting transient signals in GPS position time-series: smoothing and principal component analysis. *Geophysical Journal International*, doi: 10.1093/gji/ggt003.
- Jiang, Y., Wdowinski, S., Dixon, T.H., Hackl, M., Protti, M., Gonzalez, V., 2012. Slow slip events in Costa Rica detected by continuous GPS observations, 2002–2011. *Geochemistry Geophysics Geosystems*, doi: 10.1029/2012GC004058.
- Jin, S., Wang, J., Park, P.-H., 2005. An improvement of GPS height estimations: stochastic modeling. *Earth Planets Space* 57.
- Jin, S., Luo, O., Park, P., 2008. GPS observations of the ionospheric F2-layer behavior during the 20th November 2003 geomagnetic storm over South Korea. *Journal of Geodesy*, ISSN 0949-7714, doi: 10.1007/s00190-008-0217-x.
- Jin, S., van Dam, T., Wdowinski, S., 2013. Observing and understanding the Earth system variations from space geodesy. *Journal of Geodynamics*, <http://dx.doi.org/10.1016/j.jog.2013.08.001>, ISSN 0264-3707, in press.
- Jin, S.G., Luo, O., Ren, C., 2010. Effects of physical correlations on long-distance GPS positioning and zenith tropospheric delay estimates. *Advances in Space Research*, <http://dx.doi.org/10.1016/j.asr.2010.01.017>.
- Johnson, H.O., Agnew, D.C., 1995. Monument motion and measurements of crustal velocities. *Geophysical Research Letters*, doi: 10.1029/95GL02661.
- LaFemina, P., Dixon, T.H., Govers, R., Norabuena, E., Turner, H., Saballo, A., Mattioli, G., Protti, M., Strauch, W., 2009. Fore-arc motion and Cocos Ridge collision in Central America. *Geochemistry Geophysics Geosystems*, doi: 10.1029/2008GC002181.

- Langbein, J., 2008. Noise in GPS displacement measurements from Southern California and Southern Nevada. *Journal of Geophysical Research*, doi: 10.1029/2007JB005247.
- Malservisi, R., Furlong, K., Dixon, T., 2001. Influence of the earthquake cycle and lithospheric rheology on the dynamics of the Eastern California shear zone. *Geophysical Research Letters*, doi: 10.1029/2001GL013311.
- Malservisi, R., Dixon, T.H., La Femina, P.C., Furlong, K.P., 2003a. Holocene slip rate of the Wasatch fault zone, Utah, from geodetic data: Earthquake cycle effects. *Geophysical Research Letters*, doi: 10.1029/2003GL017408.
- Malservisi, R., Gans, C., Furlong, K.P., 2003b. Numerical modeling of strike-slip creeping faults and implications for the Hayward fault, California. *Tectonophysics*, doi: 10.1016/S0040-1951(02)00587-5.
- Malservisi, R., Hugentobler, U., Wonnacott, R., Hackl, M., 2013. How rigid is a rigid plate? Geodetic constraint from the TrigNet CGPS network, South Africa. *Geophysical Journal International*, doi: 10.1093/gji/ggs081.
- Mao, A., Harrison, C.G.A., Dixon, T.H., 1999. Noise in GPS coordinate time series. *Journal of Geophysical Research*.
- McCaffrey, R., Qamar, A.I., King, R.W., Wells, R., Khazadze, G., Williams, C.a., Stevens, C.W., Vollick, J.J., Zwick, P.C., 2007 June. Fault locking, block rotation and crustal deformation in the Pacific Northwest. *Geophysical Journal International*, <http://dx.doi.org/10.1111/j.1365-246X.2007.03371.x>, ISSN 0956540X.
- Miller, M.M., Melbourne, T., Johnson, D.J., Sumner, W.Q., 2002. Periodic Slow Earthquakes from the Cascadia Subduction Zone. *Science* 295 (5564), 2423, doi: 10.1126/science.1071193.
- Montillet, J.-P., Tregoning, P., McClusky, S., Yu, K., 2012. Extracting white noise statistics in GPS coordinate time series. In: Abbasi, A., Giesen, N. (Eds.), EGU General Assembly Conference Abstracts. EGU General Assembly Conference Abstracts, vol. 14, p. 4768.
- Olivares, G., Teferle, F., 2013. A Bayesian Monte Carlo Markov Chain Method for Parameter Estimation of Fractional Differenced Gaussian Processes. *Signal Processing IEEE Transactions on*, <http://dx.doi.org/10.1109/TSP.2013.2245658>.
- Outerbridge, K.C., Dixon, T.H., Schwartz, S.Y., Walter, J.L., Protti, M., Gonzalez, V., Biggs, J., Thorwart, M., Rabbel, W., 2010. A tremor and slip event on the Cocos-Caribbean subduction zone as measured by a global positioning system (GPS) and seismic network on the Nicoya Peninsula, Costa Rica. *Journal of Geophysical Research*, doi: 10.1029/2009JB006845.
- Perfettini, H., Avouac, J.-P., 2007. Modeling afterslip and aftershocks following the 1992 Landers earthquake. *Journal of Geophysical Research*, doi: 10.1029/2006JB004399.
- Plattner, C., Malservisi, R., Dixon, T.H., Lafemina, P., Sella, G.F., Fletcher, J., Suarez-Vidal, F., 2007. New constraints on relative motion between the Pacific plate and Baja California microplate (Mexico) from GPS measurements. *Geophysical Journal International*, <http://dx.doi.org/10.1111/j.1365-246X.2007.03494.x>.
- Rogers, C., Dragert, H., 2003. Episodic tremor and slip on the Cascadia subduction zone: the chatter of silent slip. *Science*, <http://dx.doi.org/10.1126/science.1084783>.
- Ruegg, J.C., Campos, J., Madariaga, R., Kausel, E., de Chabalier, J.B., Armijo, R., Dimitrov, D., Georgiev, I., Barrientos, S., 2002. Interseismic strain accumulation in south central Chile from GPS measurements, 1996–1999. *Geophysical Research Letters*, doi: 10.1029/2001GL013438.
- Saballos, J.A., Malservisi, R., Connor, C.B., La Femina, P.C., Wetmore, P., 2013. Gravity and geodesy of Concepcion volcano, Nicaragua. In: Palma, J.L., Rose, W.I., Varley, N., Delgado, H. (Eds.), *Open-Vent Volcanism and Related Hazards*. Geological Society of America, Special Paper (in press).
- Savage, J.C., Lisowskim, M., 1998. Viscoelastic coupling model of the San Andreas Fault along the big bend, southern California. *Journal of Geophysical Research* 103 (B4), 7281–7292.
- Schmalzle, G., Dixon, T., Malservisi, R., Govers, R., 2006. Strain accumulation across the Carrizo segment of the San Andreas Fault, California: Impact of laterally varying crustal properties. *Journal of Geophysical Research*, doi: 10.1029/2005JB003843.
- Schmidt, D.A., Gao, H., 2010. Source parameters and time-dependent slip distributions of slow slip events on the Cascadia subduction zone from 1998 to 2008. *Journal of Geophysical Research*, doi: 10.1029/2008JB00604.
- Schwartz, S.Y., Rokosky, J.M., 2007. Slow slip events and seismic tremor at circum-Pacific subduction zones. *Reviews of Geophysics*, ISSN 8755-1209, doi: 10.1029/2006RG000208.
- Segall, P., Davis, J.L., 1997. GPS applications for geodynamics and earthquake studies. *Annual Review of Earth and Planetary Sciences*, <http://dx.doi.org/10.1146/annurev.earth.25.1.301>.
- Strang, G., Borre, K., 1997. *Linear Algebra, Geodesy, and GPS*. Wellesley-Cambridge Press, Wellesley, MA, USA.
- Szeliga, W., Melbourne, T., Santillian, V., Miller, M., 2008. GPS constraints on 34 slow slip events within the Cascadia subduction zone, 1997–2005. *Journal of Geophysical Research*, doi: 10.1029/2007JB004948.
- Tryon, M.D., 2009. Monitoring aseismic tectonic processes via hydrologic responses: an analysis of log-periodic fluid flow events at the Costa Rica outer rise. *Geology*, doi: 10.1130/G25342A.1.
- Walter, J.L., Schwartz, S.Y., Protti, J.M., Gonzalez, V., 2011. Persistent tremor within the northern Costa Rica seismogenic zone. *Geophysical Research Letters*, doi: 10.1029/2010GL045586.
- Wdowinski, S., Bock, Y., Zhang, J., Fang, P., Genrich, J., 1997. Southern California permanent GPS geodetic array: spatial filtering of daily positions for estimating coseismic and postseismic displacements induced by the 1992 Landers earthquake. *Journal of Geophysical Research*.
- Williams, S.D.P., 2003a. The effect of coloured noise on the uncertainties of rates estimated from geodetic time series. *Journal of Geodesy*, doi: 10.1007/s00190-002-0283-4.
- Williams, S.D.P., 2003b. Offsets in global positioning system time series. *Journal of Geophysical Research*, doi: 10.1029/2002JB002156.
- Williams, S.D.P., Bock, Y., Fang, P., Jamason, P., Nikolaidis, R.M., Prawirodiridjo, L., Miller, M., Johnson, D.J., 2004. Error analysis of continuous GPS position time series. *Journal of Geophysical Research*.
- Yang, Q., Wdowinski, S., Dixon, T.H., 2013. Annual variation of coastal uplift in Greenland as an indicator of variable and accelerating ice mass loss. *Geochemistry, Geophysics, Geosystems*, ISSN 1525-2027, doi: 10.1002/ggge.20089.
- Zhang, J., Bock, Y., Johnson, H., Fang, P., Williams, S., Genrich, J., Wdowinski, S., Behr, J., 1997. Southern California permanent GPS geodetic array: error analysis of daily position estimates and site velocities. *Journal of Geophysical Research* 102 (B8), 18035–18055.
- Zumberge, J.F., Heflin, M.B., Jefferson, D.C., Watkins, M.M., Webb, F.H., 1997. Precise point positioning for the efficient and robust analysis of GPS data from large networks. *Journal of Geophysical Research: Solid Earth*, doi: 10.1029/96JB03860.